Ratio limits and simulation algorithms for the Palm version of stationary iterated tessellations

DAVID NEUHÄUSER*, CHRISTIAN HIRSCH*, CATHERINE GLOAGUEN** and VOLKER SCHMIDT*

* Institute of Stochastics
Ulm University, D-89069 Ulm, Germany
E-mail: david.neuhaeuser@uni-ulm.de, christian.hirsch@uni-ulm.de, volker.schmidt@uni-ulm.de
Phone: +49 731 5023532
Fax: +49 731 5023649

** Orange Labs
F-92131 Issy les Moulineaux Cedex 9, France
E-mail: catherine.gloaguen@orange.com
Phone: +33 1 45 29 64 41

Abstract

Distributional properties and a simulation algorithm for the Palm version of stationary iterated tessellations are considered. In particular we study the limit behavior of functionals related to Cox-Voronoi cells (such as typical shortest path lengths) if either the intensity γ_0 of the initial tessellation or the intensity γ_1 of the component tessellation converges to 0. We develop an explicit description of the Palm version of Poisson-Delaunay tessellations (PDT) which provides a new direct simulation algorithm for the typical Cox-Voronoi cell based on PDT. It allows us to simulate the Palm version of stationary iterated tessellations where either the initial or component tessellation is a PDT and can furthermore be used in order to show numerically that the qualitative and quantitative behavior of certain functionals related to Cox-Voronoi cells strongly depends on the type of the underlying iterated tessellation.
Keywords : Stochastic Geometry, Stationary Iterated Tessellation, Cox Process, Palm Measure, PDT, Direct Simulation Algorithm, Shortest Path Length, Ratio Limits.
2010 *Mathematics Subject Classification*: 60D05; 65C99

1 Introduction

In [6] it is shown that iterated tessellations arouse much better fits considering the underlying infrastructure and road system in telecommunication networks than simple (non-iterated) tessellations of Poisson type do. Consequently, we can also expect even better results for modeling access networks than those obtained in [7]. This paper consistently extends results on shortest-path lengths in

typical serving zones based on iterated random tessellations which have recently been derived in [17] (see also [5, 4, 12] for further results on this type of network characteristics). In particular, we investigate stochastic models for a hierarchical two-level network, i.e. path connections between two different kinds of network nodes, say high-level components (HLC) representing antennas, nodes of higher order, etc. and low-level components (LLC) such as nodes of lower order or subscribers. For modeling the locations of these nodes, we place Poisson points along the edge set of a planar iterated tessellation T representing the road system. In order to describe the connection rules between nodes within our telecommunication network model, we say that each LLC is linked to its closest HLC with respect to the Euclidean distance.
In other words, we construct the Voronoi tessellation $\{\Xi_{H,i}\}_{i\geq 1}$ with respect to the locations of the HLC $\{X_{H,i}\}_{i\geq 1}$ and associate each LLC located within the cell $\Xi_{H,i}$ with the corresponding nucleus and HLC $X_{H,i}$. The cell $\Xi_{H,i}$ is called serving zone of $X_{H,i}$. In this paper, we show the intuitive limit result that fixing the intensity γ_0 of the initial tessellation and letting the intensity γ_1 of the component tessellation converge to 0 should lead to the same distribution for functionals related with the Cox-Voronoi cells $\Xi_{H,i}$ (such as the typical shortest path length C^*) as if one replaces the underlying iterated tessellation by its initial tessellation (analogously for fixing γ_1, letting $\gamma_0 \to 0$ and considering the component tessellation). However, it is not clear how to obtain analytical results for such functionals when neither γ_0 nor γ_1 are close to 0. Therefore we develop a simulation algorithm for the Palm version T^* of an iterated tessellation T, provided that we can simulate the Palm versions of the initial and the component tessellation, in order to study the behavior of these functionals numerically. Especially a direct simulation algorithm for the Palm version of a Poisson-Delaunay tessellation is given in this context.
The paper is organized as follows. In Section 2 we briefly describe the Stochastic Subscriber Line Model and tools of stochastic geometry, especially some essential results of Palm calculus which are required for the network model investigated in the present paper. Section 3 deals with limit ratios of the intensities γ_0 and γ_1 of the initial and component tessellations. A simulation algorithm for the Palm version T^* of an iterated tessellation T is given in Section 4 in order to simulate the typical Cox-Voronoi cell based on T^*. Special emphasis is put on the explicit form of the Palm measure of a Poisson-Delaunay tessellation (PDT) which provides us with a new direct simulation algorithm for T^* when a PDT is involved. Then, in Section 5, we derive analytical functions approximating the densities of the typical shortest path length C^* and give some numerical results. Finally, Section 6 concludes the paper and gives an outlook to possible future research.

2 Mathematical preliminaries

2.1 The Stochastic Subscriber Line Model

In order to model huge and complex wired telecommunication networks such as the network of Paris, *Orange Labs* uses the *Stochastic Subscriber Line Model* (SSLM) which has been developed in the last years and is still extended. The SSLM consists of three parts which can all be modeled by means of stochastic geometry and are described in the following. Tessellations as representation for the infrastructure, point processes which model locations of subscribers as well as some basic notions and results of Palm calculus are described within this section.

2.1.1 Geometry Model - Nested iterated tessellations

The first component of the SSLM is the geometry model where the infrastructure system, i.e. the roads of a city or a town (note that the cable system is installed along the roads in order to reach each customer) are represented by random tessellations. We call a subdivision of the Euclidean space $\mathbb{R}^2$ into a sequence $\Xi_1, \Xi_2, \ldots$ of random convex and compact polygons fulfilling

(i) $\operatorname{int} \Xi_i \cap \operatorname{int} \Xi_j = \emptyset$ for $i \neq j$,

(ii) $\bigcup_{i=1}^{\infty} \Xi_i = \mathbb{R}^2$,

(iii) $\#\{i : \Xi_i \cap B \neq \emptyset\} < \infty$ for each bounded $B \subset \mathbb{R}^2$,

a (planar) random tessellation T where $T^{(1)} = \bigcup_{n=1}^{\infty} \partial\Xi_n$ denotes the union of the cell boundaries $\partial\Xi_n$ of T. For further details on random tessellations and random closed sets the reader can consult [10, 13, 14].
In this paper the focus is put on iterated tessellations (see Figure 1). For some initial tessellation $T_0 = \{\Xi_{0n}\}$ and a sequence $T_1, T_2, \ldots$ of independent and identically distributed component tessellations which are also independent of T_0, the iterated tessellation $T = \tau(T_0 \mid T_1, T_2, \ldots)$ is defined as follows: For all $n \geq 1$, the cell Ξ_{0n} of T_0 is subdivided with component tessellation T_n, i.e. the edge set $T^{(1)}$ of the iterated tessellation T is given by $T^{(1)} = \bigcup_{n=1}^{\infty} \partial\Xi_{0n} \cup (\Xi_{0n} \cap T_n^{(1)})$ where the edge set $T_0^{(1)}$ can be interpreted as main streets, and $\Xi_{0n} \cap T_n^{(1)}$ for $n \geq 1$ as side streets. In particular, the cell of T_0 which contains the origin is called zero-cell of T_0 and is denoted by Ξ_{01}. We assume that T_0 and $T_1, T_2, \ldots$ are stationary. Then $T = \tau(T_0 \mid T_1, T_2, \ldots)$ is also stationary and the intensity $\gamma = \mathbb{E}\nu_1(T^{(1)} \cap [0,1]^2)$ of T is given by $\gamma = \gamma_0 + \gamma_1$ where $\gamma_0 = \mathbb{E}\nu_1(T_0^{(1)} \cap [0,1]^2)$ and $\gamma_1 = \mathbb{E}\nu_1(T_1^{(1)} \cap [0,1]^2)$ denote the intensities of T_0 and T_1, respectively, and ν_1 is the 1-dimensional Hausdorff measure in $\mathbb{R}^2$. Well-known examples of random tessellations which are used in this paper for iteration are Poisson-line tessellations (PLT), Poisson-Voronoi tessellations (PVT) and Poisson-Delaunay tessellations (PDT) (see [1]). We say that an iterated tessellation is of type A/B if the initial tessellation is of type

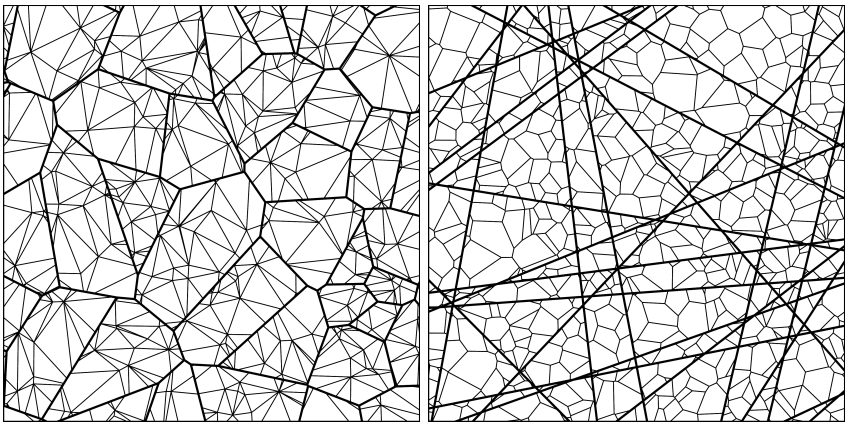

Fig. 1: Realisations of iterated tessellations: PVT/PDT (left) and PLT/PVT (right)

A and the component tessellation is of type B, e.g. PVT/PDT. Note that for simplicity, we assume in this paper that all component tessellations are of the same type which is, of course, no necessary restriction for iterated tessellations. For instance, it is possible to iterate only some cells of T_0 with a certain type of component tessellation whereas others remain empty (Bernoulli-nesting) or are filled with another type of tessellation (multi-type-nesting).
Furthermore, we define $T_0' = \gamma_0 T_0$ and $T_n' = \gamma_1 T_n$ for each $n \geq 1$, where $\mathbb{E}\nu_1(T_0'^{(1)} \cap [0,1]^2) = \mathbb{E}\nu_1(T_n'^{(1)} \cap [0,1]^2) = 1$. Note that the standardized tessellations T_0' and T_n' can be used to construct two families $(T_0(\gamma_0))_{\gamma_0>0}$ and $(T_n(\gamma_1))_{\gamma_1>0}$ of intial and component tessellations T_0 and T_n by scaling, i.e., $(T_0(\gamma_0))_{\gamma_0>0} = (T_0'/\gamma_0)_{\gamma_0>0}$ as well as $(T_n(\gamma_1))_{\gamma_1>0} = (T_n'/\gamma_1)_{\gamma_1>0}$, where the length intensities of $T_0(\gamma_0)$ and $T_n(\gamma_1)$ are given by γ_0 and γ_1, respectively. In the following we always assume that T_0 and T_n are given by scaling of some standardized tessellations, T_0' and T_n'.

2.1.2 Network model - Cox processes representing network nodes

The placement of network nodes builds up the second part of the SSLM. For the network model, we consider stationary Coxian point processes $X_H = \{X_{H,i}\}$ and $X_L = \{X_{L,i}\}$ in order to model the locations of HLC and LLC (see Figure 2). Their random intensity measures are concentrated on the edge set $T^{(1)}$ of some stationary tessellation T and are proportional to the one–dimensional Hausdorff measure ν_1 on $T^{(1)}$, i.e., $\mathbb{E}X_H(B) = \lambda_\ell \, \mathbb{E}\nu_1(B \cap T^{(1)})$ and $\mathbb{E}X_L(B) = \lambda_\ell' \, \mathbb{E}\nu_1(B \cap T^{(1)})$ for each Borel set $B \subset \mathbb{R}^2$ and for some (linear) intensities $\lambda_\ell, \lambda_\ell' > 0$. Note that the planar intensities of X_H and X_L are given by $\lambda = \lambda_\ell \gamma$ and $\lambda' = \lambda_\ell' \gamma$. For more details on (marked) Coxian point processes see e.g. [3, 14, 8].

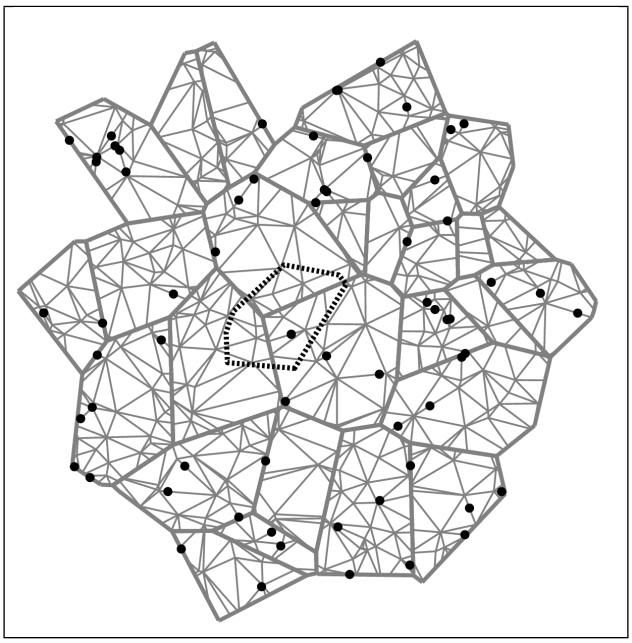

Fig. 2: Cox-Voronoi cell $\Xi_{H,i}$ (dashed) based on PVT/PDT (gray)

2.1.3 Topology Model - Cox-Voronoi cells as serving zones

The third component of the SSLM is the topology model where the serving zones of HLC are added to the telecommunication network model. In particular, we consider the Cox-Voronoi tessellation $T_H = \{\Xi_{H,i}\}$ induced by the points $X_{H,i}$ of the Cox process $X_H = \{X_{H,i}\}$ on the edge set of $T = \tau(T_0 \mid T_1, T_2, \ldots)$, i.e.

$$\Xi_{H,i} = \{x \in \mathbb{R}^2 : |x - X_{H,i}| \leq |x - X_{H,j}| \text{ for all } j \neq i\},$$

where $|\cdot|$ denotes the Euclidean norm. In this way, every HLC whose location is represented by a Cox point $X_{H,i}$ is linked with his serving zone represented by $\Xi_{H,i}$. Let us furthermore denote by $S_{H,i} = T^{(1)} \cap \Xi_{H,i}$ the segment system of the serving zone $\Xi_{H,i}$ corresponding to $X_{H,i}$. We then link each point $X_{L,i}$ of X_L to the point $X_{H,j}$ of X_H if and only if $X_{L,i} \in \Xi_{H,j}$ and mark $X_{L,i}$ with the shortest path length C_i from $X_{L,i}$ to $X_{H,j}$ along $T^{(1)}$. In this way we obtain the stationary marked point process $X_{L,C} = \{(X_{L,i}, C_i)\}$.

2.2 Palm calculus and typical serving zones

For telecommunication networks, one important cost functional we are interested in is the typical shortest path length C^* which is defined as the typical

mark of $X_{L,C}$ with representation formula

$$\mathbb{E}h(C^*) = \frac{1}{\lambda'}\,\mathbb{E}\sum_{i:\,X_{L,i}\in[0,1]^2} h(C_i)\,, \tag{1}$$

where $h : [0,\infty) \to [0,\infty)$ is an arbitrary measurable function. Although this definition makes sense from a conceptual point of view, it is difficult to efficiently compute the distribution of C^* using (1). Therefore, in order to obtain a representation formula which is easier to handle, we first have to have a look on the Palm version of the stationary Cox process X_H of the HLC, which is a point process X_H^* in the Euclidean plane $\mathbb{R}^2$ whose distribution can be given by the representation formula

$$\mathbb{E}h(X_H^*) = \frac{1}{\lambda}\,\mathbb{E}\sum_{i:\,X_{H,i}\in[0,1]^2} h(\{X_{H,n}\} - X_{H,i})\,,$$

where $h : \mathbb{N} \to [0,\infty)$ is an arbitrary measurable function and $\mathbb{N}$ denotes the family of all locally finite sets of $\mathbb{R}^2$. Note that $\mathbb{P}(o \in X_H^*) = 1$ by definition, where the distribution of X_H^* is called the Palm distribution of X_H which can be interpreted as conditional distribution of X_H given that there is a point located at the origin. In addition, the reduced Palm version $X_H^* \setminus \{o\}$ of X_H is a Cox process, too. The random intensity measure Λ^* of $X_H^* \setminus \{o\}$ is given by $\Lambda^*(B) = \lambda_\ell\,\nu_1(T^{*(1)} \cap B)$ for each Borel set $B \subset \mathbb{R}^2$ and for T^*, the Palm version of T, whose distribution is given by

$$\mathbb{E}h(T^*) = \frac{1}{\gamma}\,\mathbb{E}\int_{T^{(1)}\cap\,[0,1]^2} h(T-x)\,\nu_1(dx)\,, \tag{2}$$

where $h : \mathbb{T} \to [0,\infty)$ is an arbitrary measurable function and $\mathbb{T}$ denotes the family of all tessellations in $\mathbb{R}^2$. Note that $\mathbb{P}(o \in T^{*(1)}) = 1$ by definition, where the distribution of T^* can be interpreted as conditional distribution of T given that the origin o belongs to an edge of T. The typical Voronoi cell Ξ_H^* of X_H is defined as the Voronoi cell at o with respect to X_H^*. Furthermore, the typical segment system S_H^* is then defined as the typical mark of the Coxian point process of the HLC $X_{H,i}$ marked with the corresponding segment systems $S_{H,i}$. This provides the following representation formula for the distribution of the typical shortest path length C^* which has been derived in [12]. It holds that

$$\mathbb{E}h(C^*) = \lambda_\ell \mathbb{E}\int_{S_H^*} h(c(y))\nu_1(dy), \tag{3}$$

where $h : [0,\infty) \to [0,\infty)$ is an arbitrary measurable function and $c(y)$ denotes the shortest path length from $y \in S_H^*$ to the origin o along the edges of S_H^*. For more details on typical shortest path lengths and typical segment systems, the reader is referred to [7] and [12] again.

3 Limit theorems

3.1 Some auxiliary results

In order to find out similarities and differences for the distributional behavior of C^* based on simple and iterated tessellations, respectively, we begin by considering the limit cases $\gamma_0 \to 0$ where γ_1 is fixed and vice versa. The mindful reader may expect that the more the intensity of either T_0 or T_n is reduced, the more the typical shortest path length based on an iterated tessellation behaves like the typical shortest path length based on the corresponding simple (non-iterated) tessellation. Indeed, we show this formally in this section. In [17] the following representation formula has been derived for T^*. For an arbitrary measurable function $h : \mathbb{T} \mapsto [0, \infty)$, it holds that

$$\mathbb{E}h(T^*) = \frac{\gamma_0}{\gamma}\,\mathbb{E}h(\tau(T_0^* \mid T_1, T_2, \ldots)) + \frac{\gamma_1}{\gamma}\,\mathbb{E}h(\tau(T_0 \mid T_1^*, T_2, T_3, \ldots)), \tag{4}$$

where the component tessellations T_1 and T_1^* subdivide the zero-cell of T_0^* and T_0, respectively. Let X_H^I and X_H^C denote Cox processes whose random intensity measures are given by $\lambda_\ell \nu_1(\cdot \cap \tau(T_0^* \mid T_1, T_2, \ldots))$ and $\lambda_\ell \nu_1(\cdot \cap \tau(T_0 \mid T_1^*, T_2, T_3, \ldots))$ respectively. In addition, we write $X_{H,o}^I$ and $X_{H,o}^C$ for the closest point to the origin (in the Euclidean sense) of X_H^I and X_H^C, respectively. Considering the typical shortest-path length C^*, we can use (4) to obtain the following result.

Lemma 3.1. *Let $h : [0, \infty) \to [0, \infty)$ be a measurable function. Then*

$$\mathbb{E}h(C^*) = \frac{\gamma_0}{\gamma}\mathbb{E}h(C_0^*) + \frac{\gamma_1}{\gamma}\mathbb{E}h(C_1^*),$$

where $C_0^* = c(X_{H,o}^I)$ and $C_1^* = c(X_{H,o}^C)$ denotes the shortest path length from $X_{H,o}^I$ and $X_{H,o}^C$ to the origin along the edges of $\tau(T_0^* \mid T_1, T_2, \ldots)$ and $\tau(T_0 \mid T_1^*, T_2, T_3, \ldots)$, respectively.

Proof. For a deterministic tessellation t such that $o \in t^{(1)}$ we define $f(t) = \mathbb{E}\left(h\left(c(X_{H,o}^t)\right)\right)$, where $X_{H,o}^t$ denotes the closest point to the origin of some Poisson process X_H^t on $t^{(1)}$. Then we compute

$$\begin{aligned}
&\mathbb{E}h(C^*) = \mathbb{E}\left(\mathbb{E}\left(h(C^*) \mid T^*\right)\right) = \mathbb{E}f(T^*)\\
&= \frac{\gamma_0}{\gamma}\,\mathbb{E}f(\tau(T_0^* \mid T_1, T_2, \ldots)) + \frac{\gamma_1}{\gamma}\,\mathbb{E}f(\tau(T_0 \mid T_1^*, T_2, T_3, \ldots))\\
&= \frac{\gamma_0}{\gamma}\mathbb{E}(\mathbb{E}(h(C_0^*) \mid \tau(T_0^* \mid T_1, T_2, \ldots))) + \frac{\gamma_1}{\gamma}\mathbb{E}(\mathbb{E}(h(C_1^*) \mid \tau(T_0 \mid T_1^*, T_2, T_3, \ldots)))\\
&= \frac{\gamma_0}{\gamma}\mathbb{E}h(C_0^*) + \frac{\gamma_1}{\gamma}\mathbb{E}h(C_1^*),
\end{aligned}$$

where we used (4) in the third equality. □

Lemma 3.2. *Let $T \subset \mathbb{R}^2$ be a stationary random tessellation with intensity γ. Denote by X a Cox process on $T^{*(1)}$ with linear intensity λ_ℓ. Denote by $X_o \in X$ the closest point of X to the origin o. For $n \geq 1$ denote by $A_n^{(1)}$ the event that $c(X_o) < n$. Then $\mathbb{P}(A_n^{(1)}) \to 1$ as $n \to \infty$.*

Proof. The claim immediately follows from the fact that $\lim_{n\to\infty} \mathbb{P}(A_n^{(1)}) = \mathbb{P}(c(X_o) < \infty) = 1$. □

3.2 The case $\gamma_0 \to 0$

We begin by considering the case $\gamma_0 \to 0$ where γ_1 is fixed. A realisation of $T = \tau(T_0 \mid T_1, T_2, \ldots)$ where T_0 is a PVT and T_1 is a PLT such that γ_0 is close to zero (but γ_1 not) is shown in Figure 3.

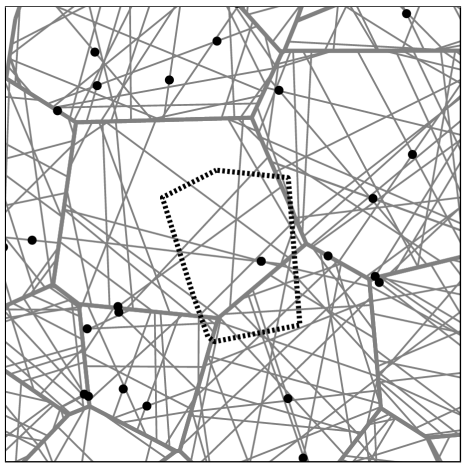

Fig. 3: PVT/PLT where $\gamma_0 \to 0$

Lemma 3.3. *Let $\gamma_0 > 0$ and $n \geq 1$. Furthermore, write $A_{n,\gamma_0}^{(2)}$ for the event that the zero-cell of the tessellation $T_0 = T_0(\gamma_0)$ contains the ball $B_n(o)$ centered at the origin $o \in \mathbb{R}^2$ with radius n. Then, for each $n \geq 1$ it holds that $\mathbb{P}(A_{n,\gamma_0}^{(2)}) \to 1$ as $\gamma_0 \to 0$.*

Proof. Denote by Ξ'_{01} the zero-cell of the standardized tessellation T'_0 and by $\Xi_{01} = \Xi'_{01}/\gamma_0$ the zero-cell of the tessellation $T_0 = T_0(\gamma_0)$. The claim now follows immediately from the fact that $\mathbb{P}(o \in \operatorname{int} \Xi'_{01}) = 1$ and, therefore, $\bigcup_{\gamma_0>0} \Xi'_{01}/\gamma_0 = \mathbb{R}^2$ a.s. □

Observe that each pair of Cox processes with the same (linear) intensity λ_ℓ whose random intensity measures are concentrated on $T_1^{*(1)}$ and $\tau(T_0 \mid T_1^*, T_2, T_3, \ldots)^{(1)}$, respectively, can be coupled so that they coincide in the interior of the zero-cell of the initial tessellation T_0. Denote by $A_{\gamma_0}^{(3)}$ the event that in this coupling the

shortest paths to the closest point to the origin of the Cox processes on $T_1^{*(1)}$ and $\tau(T_0 \mid T_1^*, T_2, T_3, \ldots)^{(1)}$ coincide.

Lemma 3.4. *It holds that* $\mathbb{P}(A_{\gamma_0}^{(3)}) \to 1$ *as* $\gamma_0 \to 0$.

Proof. The assertion immediately follows from Lemmas 3.2 and 3.3. □

Proposition 3.5. *Let* $h : [0,\infty) \to [0,\infty)$ *be a bounded measurable function and fix* $\gamma_1 > 0$. *Then* $\mathbb{E}h(C^*) \to \mathbb{E}h(C_{comp}^*)$ *as* $\gamma_0 \to 0$ *where* C_{comp}^* *denotes the typical shortest path length based on the (non-iterated) component tessellation* T_1. *In particular,* C^* *converges in distribution to* C_{comp}^* *as* $\gamma_0 \to 0$.

Proof. By Lemma 3.1 it suffices to prove that $\mathbb{E}h(C_1^*) \to \mathbb{E}h(C_{comp}^*)$ as $\gamma_0 \to 0$. Observe that

$$\begin{aligned}\mathbb{E}h(C_1^*) &= \mathbb{E}(h(C_1^*)\mathbb{1}_{A_{\gamma_0}^{(3)}}) + \mathbb{E}(h(C_1^*)(1-\mathbb{1}_{A_{\gamma_0}^{(3)}})) \\ &= \mathbb{E}(h(C_{comp}^*)\mathbb{1}_{A_{\gamma_0}^{(3)}}) + \mathbb{E}(h(C_1^*)(1-\mathbb{1}_{A_{\gamma_0}^{(3)}})) \\ &= \mathbb{E}h(C_{comp}^*) + \mathbb{E}(h(C_1^*)(1-\mathbb{1}_{A_{\gamma_0}^{(3)}})) + \mathbb{E}(h(C_{comp}^*)(\mathbb{1}_{A_{\gamma_0}^{(3)}}-1)),\end{aligned}$$

where $\mathbb{1}_{A_{\gamma_0}^{(3)}}$ denotes the indicator of $A_{\gamma_0}^{(3)}$. Taking into account that the function $h : [0,\infty) \to [0,\infty)$ is bounded, Lemma 3.4 implies that the last two summands of this expression tend to zero as $\gamma_0 \to 0$. This proves the result. □

Remark 1. *Let* T *be a stationary tessellation of intensity* γ *and for* $\gamma > 0$ *denote by* $C^*(\gamma)$ *the typical shortest path length for the tessellation* T/γ. *Observe that the distribution of* $C^*(\gamma)$ *satisfies the scaling relation* $C^*(1) \stackrel{d}{=} \gamma\, C^*(\gamma)$. *In particular, by Slutsky's lemma, Proposition 3.5 remains true if we relax the assumption that* γ_1 *is constant (say* $\gamma_1 = c$*) and* $\gamma_0 \to 0$ *by* $\gamma_1 = c - \gamma_0$ *and* $\gamma_0 \to 0$.

3.3 The case $\gamma_1 \to 0$

Now let us deal with the limiting case where γ_0 is fixed and $\gamma_1 \to 0$. A realisation of $T = \tau(T_0 \mid T_1, T_2, \ldots)$ where T_0 is a PVT and T_1 is a PLT such that γ_1 is close to zero (but γ_0 is not) is shown in Figure 4.
The arguments given below are similar to those of the case $\gamma_0 \to 0$ considered in Section 3.2 but we present the details for the convenience of the reader. By Lemma 3.1 it suffices to prove that $\mathbb{E}h(C_0^*) \to \mathbb{E}h(C_{init}^*)$ where C_{init}^* denotes the typical shortest path length based on the (non-iterated) initial tessellation T_0.

Lemma 3.6. *Let* $\gamma_1 > 0$ *and* $n \geq 1$. *Let furthermore* $A_{n,\gamma_1}^{(4)}$ *denote the event that* $(\tau(T_0^* \mid T_1, T_2, \ldots))^{(1)} \cap B_n(o) = T_0^{*(1)} \cap B_n(o)$. *Then, for each* $n \geq 1$, *it holds that* $\lim_{\gamma_1 \to 0} \mathbb{P}(A_{\gamma_1,n}^{(4)}) = 1$.

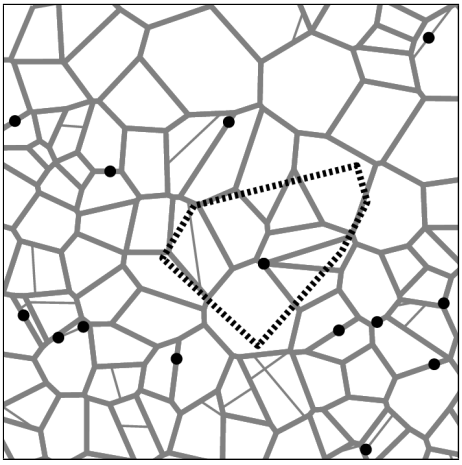

Fig. 4: PVT/PLT where $\gamma_1 \to 0$

Proof. Denote by $\Xi_{0,m_1}, \dots, \Xi_{0,m_k}$ the cells of T_0^* that intersect $B_n(o)$. Furthermore, given T_0^*, denote by $\Xi'_{m_j,1}$ the zero-cell of the m_j-th standardized component tessellation T'_{m_j}. Then, for each $1 \le j \le k$ we have $\mathbb{P}(o \in \operatorname{int} \Xi'_{m_j,1}) = 1$ and therefore

$$\bigcup_{\gamma_1>0} \bigcap_{j=1}^{k} \Xi'_{m_j,1}/\gamma_1 = \mathbb{R}^2 \text{ a.s.}$$

which proves the lemma. □

Observe that similar to Section 3.2, each pair of Cox processes with the same (linear) intensity λ_ℓ whose random intensity measures are concentrated on $T_0^{*(1)}$ and $\tau(T_0^* \mid T_1, T_2, \dots)^{(1)}$, respectively, can be coupled so that they coincide on $T_0^{*(1)}$. Denote by $A_{\gamma_1}^{(5)}$ the event that in this coupling the shortest paths to the closest point to the origin of the Cox processes on $T_0^{*(1)}$ and $\tau(T_0^* \mid T_1, T_2, T_3, \dots)^{(1)}$ coincide.

Lemma 3.7. *It holds that* $\mathbb{P}(A_{\gamma_1}^{(5)}) \to 1$ *as* $\gamma_1 \to 0$.

Proof. The assertion immediately follows from Lemmas 3.2 and 3.6. □

Proposition 3.8. *Let* $h : [0,\infty) \to [0,\infty)$ *be a bounded measurable function and fix* $\gamma_0 > 0$. *Then* $\lim_{\gamma_1 \to 0} \mathbb{E}h(C^*) = \mathbb{E}h(C^*_{init})$ *as* $\gamma_1 \to 0$ *where* C^*_{init} *denotes the typical shortest-path length based on the (non-iterated) initial tessellation* T_0.

Proof. By Lemma 3.1 it suffices to prove that $\mathbb{E}h(C_0^*) \to \mathbb{E}h(C^*_{init})$. Similarly to the proof of Proposition 3.5 we get that

$$\mathbb{E}h(C_0^*) = \mathbb{E}h(C^*_{init}) + \mathbb{E}(h(C_0^*)(1 - \mathbb{1}_{A_{\gamma_1}^{(5)}})) + \mathbb{E}(h(C^*_{init})(\mathbb{1}_{A_{\gamma_1}^{(5)}} - 1)).$$

Thus, taking into account that h is bounded, Lemma 3.7 proves the result. □

Remark 2. *Again, the scaling relation* $C^*(1) \stackrel{d}{=} \gamma\ C^*(\gamma)$ *and Slutsky's lemma imply that Proposition 3.8 remains true if we relax the assumption that* γ_0 *is constant (say* $\gamma_0 = c$*) and* $\gamma_1 \to 0$ *by* $\gamma_0 = c - \gamma_1$ *and* $\gamma_1 \to 0$*.*

4 Simulation algorithms

In Section 3 we studied the limit behavior of C^* for iterated tessellations where $\gamma_i \to 0$ for $i \in \{0,1\}$ and γ_j was fixed for $j \in \{0,1\}$, $j \neq i$. We now want to investigate what happens if neither γ_0 nor γ_1 are close to 0. Since it is unclear – like in the non-iterated case – how to compute the distribution of C^* analytically, we derive an algorithm which allows us to simulate the Palm version of stationary iterated tessellations. Using this simulation algorithm, we can compute the distribution of C^* at least numerically and proceed to study its behavior for arbitrary values of γ_0 and γ_1. In [17] a simulation algorithm has been derived for the Palm version T^* of iterated tessellations T provided that the Palm versions T_0^* and T_1^* of the initial tessellation T_0 and component tessellation T_1 can be simulated. For the convenience of the reader, we just summarize the main steps of this algorithm.

1) Simulate $Z \sim U[0,1]$. If $Z < \gamma_0/\gamma$, go to step 2a, else go to step 2b.

2a) Simulate the Palm version T_0^* of the initial tessellation T_0 and subdivide its cells $\Xi_{01}^*, \Xi_{02}^*, \ldots$ by $T_1, T_2, \ldots$, respectively, which yields T^*.

2b) Simulate T_0, subdivide the zero cell Ξ_{01} of T_0 by T_1^* and subdivide the cells $\Xi_{02}, \Xi_{03}, \ldots$ of T_0 by $T_2, T_3, \ldots$, which yields T^*.

Note that this algorithm is based on the fact that the origin belongs to the edge system of T^*, where either $o \in T_0^{*(1)}$ with probability γ_0/γ or $o \in T_1^{*(1)}$ with probability γ_1/γ. In [4] and [5], direct simulation algorithms for the Palm version of PVT and PLT have been derived, which can be used within our context. The algorithm for PVT is based on an explicit description of the Palm version of PVT which was obtained in [2], whereas the algorithm for PLT is an immediate application of Slivnyak's theorem. For the Palm version of PDT so far, only an indirect simulation algorithm is known (see [15]) which works for non-iterated PDT, but as soon as PDT is involved in an iterated tessellation, this indirect algorithm unfortunately becomes useless. Applying similar techniques as in [2], we therefore derive a new direct simulation algorithm of the typical Cox-Voronoi cell with underlying PDT which is based on the following explicit description of the Palm version of PDT.

4.1 Explicit description of the Palm version of PDT

For $\varphi \subset \mathbb{R}^2$ locally finite we denote by $Del(\varphi)$ the Delaunay graph on φ, i.e., the geometric graph with vertex set φ where $x, y \in \varphi$ are connected by an

edge if and only if there exists a closed disk $B \subset \mathbb{R}^2$ with $\varphi \cap B = \{x, y\}$. For $\rho \in [-\pi/2, \pi/2]$ write $g_\rho : \mathbb{R}^2 \to \mathbb{R}^2$ for the rotation of $\mathbb{R}^2$ by angle ρ. Furthermore, for $u, v \in \mathbb{R}^2$ with $u \neq v$, write

$$L^+(u, v) = \{x \in \mathbb{R}^2 : \langle x - u, g_{\pi/2}(v - u)\rangle > 0\}$$

for the positive half-space whose boundary is determined by the ray with starting point u and direction $v-u$. For a locally finite set $\varphi \subset \mathbb{R}^2$ define $x_1(\varphi)$, $x_2(\varphi) \in \varphi$ to be the points such that $[x_1(\varphi), x_2(\varphi)]$ is an edge of the Delaunay triangulation $Del(\varphi)$ on φ containing o and such that the first coordinate of $x_1(\varphi)$ is negative (provided that such points exist). Furthermore if such points exist choose $x_3(\varphi) \in \varphi$ such that the disc $B(x_1(\varphi), x_2(\varphi), x_3(\varphi))$ containing $x_1(\varphi), x_2(\varphi), x_3(\varphi)$ on its boundary does not contain any further points of φ and such that $x_3(\varphi) \in L^+(x_1(\varphi), x_2(\varphi))$. In particular, then $x_1(\varphi), x_2(\varphi)$ and $x_3(\varphi)$ form a triangle in $Del(\varphi)$ and $o \in [x_1(\varphi), x_2(\varphi)]$ (see Figure 5). If such points do not exist, then we put $x_1(\varphi) = x_2(\varphi) = x_3(\varphi) = o$. Furthermore define $s(\varphi) = |x_1(\varphi) - x_2(\varphi)|$ to be the length of the edge in $Del(\varphi)$ which contains the origin $o \in \mathbb{R}^2$. We also put $e_1(\varphi) = (x_2(\varphi) - x_1(\varphi))/\,|x_2(\varphi) - x_1(\varphi)|$, $e_2(\varphi) = g_{\pi/2}(e_1(\varphi))$ and consider these vectors to be a basis of $\mathbb{R}^2$ which is adapted to the direction of the Delaunay edge $[x_1(\varphi), x_2(\varphi)]$. Furthermore we denote by $u_1(\varphi), u_2(\varphi)$ the coordinates of $x_3(\varphi)$ in this basis, i.e., $x_3(\varphi) = u_1(\varphi)e_1(\varphi) + u_2(\varphi)e_2(\varphi)$.

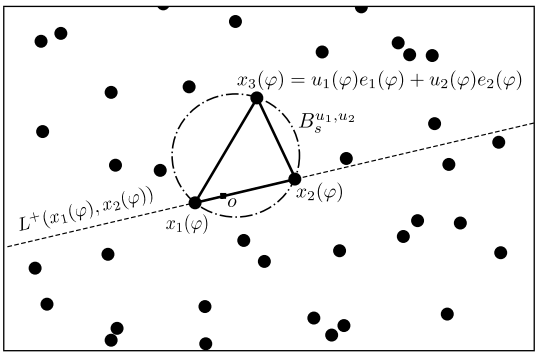

Fig. 5: Delaunay triangle through $x_1(\varphi), x_2(\varphi)$ and $x_3(\varphi)$ containing the origin

Let furthermore T^* be the Palm version of the Poisson-Delaunay triangulation T and let us write $T^{*(0)}$ for the vertex set of T^*.

Theorem 4.1. *Let $\lambda > 0$ and let $X \subset \mathbb{R}^2$ be a homogeneous Poisson process with intensity λ. Let (L, U_1, U_2) be the random vector defined by $(L, U_1, U_2) = (s(T^{*(0)}), u_1(T^{*(0)}), u_2(T^{*(0)}))$. Then, the following is true.*

1. *The joint distribution function of* (L, U_1, U_2) *is given by*

$$\mathbb{P}\left(L \leq \delta, U_1 \leq a, U_2 \leq b\right) = \\ = \frac{3\pi^2\lambda^{5/2}}{32} \int_0^{\delta} \int_{-\infty}^{a} \int_0^{b} s^2 exp\left(-\lambda\nu_2\left(B_s^{u_1,u_2}\right)\right)\, du_2\, du_1\, ds,$$

for any $\delta > 0$, $a \in \mathbb{R}$ *and* $b > 0$, *where* $B_s^{u_1,u_2} = B\left(-\frac{s}{2}e_1, \frac{s}{2}e_1, (u_1,u_2)^\top\right)$ *denotes the disc containing* $-\frac{s}{2}e_1$, $\frac{s}{2}e_1$ *and* $(u_1,u_2)^\top$ *on its boundary.*

2. *Let* ξ *be a random angle chosen uniformly from* $[-\pi/2, \pi/2]$. *Assume that* ξ *and* L *are independent and let* $W_1 = (W_{1,x}, 0)^\top$ *be a random point which is conditionally uniformly distributed in* $[-L/2, L/2]$ *given* L. *Write* $X_1' = (-L/2, 0)^\top$, $X_2' = (L/2, 0)^\top$, $X_3' = (U_1, U_2)^\top$ *and for all* $i \in \{1,2,3\}$ *define* $X_i = g_\xi(X_i' - W_1)$ *(the points* X_1, X_2, X_3 *will determine a Delaunay triangle in* $Del(T^*)$ *such that* $o \in [X_1, X_2]$*). Furthermore let* X' *denote the restriction of a homogeneous Poisson point process of intensity* λ *to* $\mathbb{R}^2 \setminus B(X_1, X_2, X_3)$, *which is conditionally independent of* (X_1, X_2, X_3). *Then,* $T^{*(0)} \stackrel{d}{=} \{X_1, X_2, X_3\} \cup X'$.

Proof. We prove parts (1) and (2) simultaneously. Let us write $\gamma = \frac{32}{3\pi}\sqrt{\lambda}$ for the length intensity of $Del(X)$. Let $f : \mathbb{N} \to [0, \infty)$ be a measurable function. For $x_1, x_2 \in \mathbb{R}^2$ we write $x_1 \leq x_2$ if the first coordinate of x_1 is less or equal the first coordinate of x_2. Using the Slivnyak-Mecke formula (see [13]) we then compute

$$\mathbb{E}(f(T^{*(0)})) = \frac{1}{\gamma}\mathbb{E}\int_{T\cap[0,1]^2} f(X - x)dx$$

$$= \frac{1}{\gamma}\mathbb{E}\sum_{\substack{X_1,X_2,X_3\in X \\ \text{pw. distinct}}} \int_{X_1}^{X_2} \mathbb{1}_{[0,1]^2}(x)\mathbb{1}_{X(B(X_1,X_2,X_3))=0,\, X_1\leq X_2,\, X_3\in L^+(X_1,X_2)} f(X - x)dx$$

$$= \frac{\lambda^3}{\gamma}\int_{\mathbb{R}^2}\int_{\mathbb{R}^2}\int_{\mathbb{R}^2}\int_{x_1}^{x_2} \mathbb{1}_{x\in[0,1]^2}\mathbb{1}_{x_1\leq x_2}\mathbb{1}_{x_3\in L^+(x_1,x_2)}$$

$$\times\, \mathbb{E}\mathbb{1}_{X(B(x_1,x_2,x_3))=0} f(\{x_1 - x, x_2 - x, x_3 - x\} \cup (X - x))dxdx_1dx_2dx_3.$$

This gives that

$$\mathbb{E}(f(T^{*(0)})) = \frac{\lambda^3}{\gamma}\int_{\mathbb{R}^2}\int_{\mathbb{R}^2}\int_{\mathbb{R}^2}\int_{o}^{x_2-x_1} \mathbb{1}_{y+x_1\in[0,1]^2}\mathbb{1}_{x_1\leq x_2}\mathbb{1}_{x_3\in L^+(x_1,x_2)}$$

$$\times\, \mathbb{E}\mathbb{1}_{(X-(x_1+y))(B(-y,x_2-x_1-y,x_3-x_1-y))=0}$$

$$\times\, f(\{-y, (x_2 - x_1) - y, (x_3 - x_1) - y\} \cup (X - (x_1 + y)))dydx_1dx_2dx_3$$

$$= \frac{\lambda^3}{\gamma}\int_{\mathbb{R}^2}\int_{\mathbb{R}^2}\int_{\mathbb{R}^2}\int_{0}^{y_2} \mathbb{1}_{y+x_1\in[0,1]^2}\mathbb{1}_{0\leq y_2}\mathbb{1}_{y_3\in L^+(0,y_2)}$$

$$\times\, \mathbb{E}\mathbb{1}_{X(B(-y,y_2-y,y_3-y))=0} f(\{-y, y_2 - y, y_3 - y\} \cup X)dydx_1dy_2dy_3,$$

where we first reparametrized the integral $\int_{x_1}^{x_2}\cdots dx$ using the substitution $y = x - x_1$, then consider the further substitutions $y_2 = x_2 - x_1$ and $y_3 = x_3 - x_1$ and

finally recalled that X is stationary. Thus an application of Fubini's theorem yields

$$\mathbb{E}(f(T^{*(0)})) = \frac{\lambda^3}{\gamma} \int_{\mathbb{R}^2} \int_{\mathbb{R}^2} \int_0^{y_2} \mathbb{1}_{0\le y_2} \mathbb{1}_{y_3 \in L^+(o,y_2)} \mathbb{E}\mathbb{1}_{X(B(-y,y_2-y,y_3-y))=0} \times f(\{-y, y_2-y, y_3-y\} \cup X) dy dy_2 dy_3.$$

Next we use the substitutions $y_2 = s g_\rho(e_1)$, $w = y - y_2/2$ and $z_4 = w + y_3 - y$ to obtain

$$\mathbb{E}(f(T^{*(0)})) = \frac{\lambda^3 \pi}{\gamma} \int_0^\infty \int_{\mathbb{R}^2} \int_{-\frac{s}{2} g_\rho(e_1)}^{\frac{s}{2} g_\rho(e_1)} \frac{1}{\pi} \int_{-\pi/2}^{\pi/2} s \mathbb{1}_{z_4 \in L^+(o, g_\rho(e_1))} \times \mathbb{E}\mathbb{1}_{X(B(-\frac{s}{2} g_\rho(e_1)-w, \frac{s}{2} g_\rho(e_1)-w, z_4-w))=0} \times f(\{-\frac{s}{2} g_\rho(e_1) - w, \frac{s}{2} g_\rho(e_1) - w, z_4 - w\} \cup X) d\rho dw dz_4 ds.$$

These integrals can be made more explicit by using the substitutions $w_1 = g_{-\rho}(w)$ and $(u_1, u_2) = g_{-\rho}(z_4)$.

$$\mathbb{E}(f(T^{*(0)})) = \frac{\lambda^3 \pi}{\gamma} \int_0^\infty \int_{-\infty}^\infty \int_0^\infty \frac{1}{s} \int_{(-s/2,0)}^{(s/2,0)} \frac{1}{\pi} \times \int_{-\pi/2}^{\pi/2} s^2 \mathbb{E}\mathbb{1}_{X(g_\rho(B((-s/2,0)-w_1, (s/2,0)-w_1, (u_1,u_2)-w_1)))=0} \times f(g_\rho(\{(-s/2,0)-w_1, (s/2,0)-w_1, (u_1,u_2)-w_1\}) \cup X) d\rho dw_1 du_2 du_1 ds$$

Finally using the formula for the void probabilities of a homogeneous Poisson point process $X \subset \mathbb{R}^2$ with intensity $\lambda > 0$, we compute

$$\mathbb{E}(f(T^{*(0)})) = \frac{\lambda^3 \pi}{\gamma} \int_0^\infty \int_{-\infty}^\infty \int_0^\infty \frac{1}{s} \int_{(-s/2,0)}^{(s/2,0)} \frac{1}{\pi} \int_{-\pi/2}^{\pi/2} s^2 \times \exp(-\lambda \nu_2(B((-s/2,0)-w_1, (s/2,0)-w_1, (u_1,u_2)-w_1))) \mathbb{E}\Big(f(g_\rho(\{(-s/2,0)-w_1, (s/2,0)-w_1, (u_1,u_2)-w_1\}) \cup \widetilde{X}) \mid \widetilde{X}(g_\rho(B((-s/2,0)-w_1, (s/2,0)-w_1, (u_1,u_2)-w_1))) = 0 \Big) d\rho dw_1 du_2 du_1 ds,$$

where $\widetilde{X} \subset \mathbb{R}^2$ is a homogeneous Poisson point process with intensity $\lambda > 0$. Observe that the distribution of X' is the same as the distribution of a homogeneous Poisson point process $\widetilde{X}$ of intensity λ conditioned on the event $\widetilde{X}(B(X_1, X_2, X_3)) = 0$. As this computation is valid for all measurable functions $f : \mathbb{N} \to [0, \infty)$ this proves the claim. □

4.2 Acceptance-rejection scheme

As explained in [4], the explicit description of the Palm version of PVT can be easily transferred into a direct simulation algorithm. Unfortunately it is not

clear how to directly draw random vectors (L, U_1, U_2) with the (joint) density $f(s,u_1,u_2) = \frac{\pi\lambda^3}{\gamma} s^2 \exp\left(-\lambda\nu_2\left(B_s^{u_1,u_2}\right)\right)$ which has been derived in Theorem 4.1. Nevertheless, this goal can be achieved by a simple acceptance-rejection scheme (see e.g. [9] for a detailed introduction to this sampling-method). To be more precise we consider a constant $c > 0$ and a probability density $g(s,u_1,u_2)$ with $f(s,u_1,u_2) \leq c \cdot g(s,u_1,u_2)$ for any $(s,u_1,u_2) \in [0,\infty) \times \mathbb{R} \times [0,\infty)$ and with the property that a sampling scheme for a random vector with density g is known. By geometric arguments it follows that

$$\nu_2(B_s^{u_1,u_2}) \geq \max\{\pi(s/2)^2, su_2/2, s\,|u_1|\}$$

and thus we obtain

$$\begin{aligned} & s^2 \exp\left(-\lambda\nu_2\left(B_s^{u_1,u_2}\right)\right) \\ & \leq \exp\left(-\pi\lambda/3(s/2)^2\right) \cdot s \cdot \exp(-\lambda(su_2/6)) \cdot s \cdot \exp(-\lambda(s\,|u_1|\,/3))). \end{aligned} \tag{5}$$

This means a dominating density function $g(s,u_1,u_2)$ can be constructed by first drawing s as the absolute value of a normally distributed random variable S and conditional on the value of $S = s$ drawing $|u_1|$ and u_2 as realisations of certain exponentially distributed random variables V_1 and V_2. Considering the arguments of each of the three exponential functions on the right hand side of (5), we get $\mu = 0$ and $\sigma^2 = \frac{6}{\pi\lambda}$ as parameters for the $N(\mu,\sigma^2)$-distributed random variable S and $\eta = \frac{\lambda s}{3}$ and $\theta = \frac{\lambda s}{6}$ for the exponentially distributed random variables V_1 and V_2 with parameters η and θ, respectively. We now have to find $c > 0$ such that

$$\begin{aligned} f(s,u_1,u_2) &= \frac{\pi\lambda^3}{\gamma} s^2 \exp\left(-\lambda\nu_2\left(B_s^{u_1,u_2}\right)\right) \\ &\leq c \cdot \alpha_1 \exp(-\frac{\lambda\pi}{12}s^2) \cdot \alpha_2 s\, \exp(-\frac{\lambda s u_2}{6}) \cdot \alpha_3 s\, \exp(-\frac{\lambda s|u_1|}{3}) \\ &= c \cdot g(s,u_1,u_2) \end{aligned}$$

and therefore it suffices to find $c > 0$ such that $\frac{\pi\lambda^3}{\gamma} \leq c \cdot \alpha_1\alpha_2\alpha_3$. Reconsidering the parameters for the three distributions, we obtain $\alpha_1 = \sqrt{\frac{\lambda}{3}}$,$\alpha_2 = \frac{\lambda}{6}$ and $\alpha_3 = \frac{\lambda}{3}$ so that we finally get $c \geq \frac{18\pi\sqrt{3\lambda}}{\gamma}$.
Summarizing the results derived in this section, we get the following simulation algorithm for the Palm version T^* of a PDT T where $T^{*(1)}$ contains the origin o:

1. Set $i = 1$
2. Simulate the random vector $(S, V_1, V_2)_i$ where
   (i) $S \sim N(0, \frac{6}{\pi\lambda})$
   (ii) $V_1 \sim Exp(\frac{\lambda s}{3})$

(iii) $V_2 \sim Exp(\frac{\lambda s}{6})$

3. Simulate $Z_i \sim U(0,1]$ and for $h(x,y,z) = \frac{f(x,y,z)}{g(x,y,z)}$, calculate $\frac{h((S,V_1,V_2)_i)}{c} = \exp\Big(\frac{\pi\lambda}{12}s^2 + \frac{\lambda s u_2}{6} + \frac{\lambda s|u_1|}{3} - \lambda\nu_2\,(B_s^{u_1,u_2})\Big)$

4. If $Z_i \geq \frac{h((S,V_1,V_2)_i)}{c}$, set $i = i+1$ and go to step 2;
else put $I = i$, i.e. $I = \min\{i \geq 1 : Z_i < \frac{h((S,V_1,V_2)_i)}{c}\}$ and determine $Y = (S,V_1,V_2)_I \sim F$ where F is the corresponding distribution function of $f(s,u_1,u_2)$ from which we want to draw random vectors

5. Put $x_1' = (-\frac{s}{2},0)^\top$, $x_2' = (\frac{s}{2},0)^\top$ and $x_3' = (u_1,u_2)^\top$ which form the first Delaunay triangle (see Figure 6)

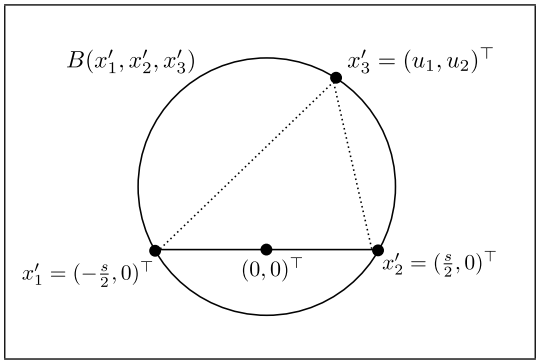

Fig. 6: Starting Delaunay triangle containing the origin

6. Rotate the Delaunay triangle with a $U[-\pi/2, \pi/2]$-distributed random angle ρ, simulate $R \sim U[-1,1]$ and add $R \cdot x_1'$ to x_1',x_2' and x_3' respectively in order to place the origin uniformly distributed on the segment between x_1' and x_2'. This transforms our original triangle $\Delta(x_1', x_2', x_3')$ to the new triangle $\Delta(x_1, x_2, x_3)$ (see Figure 7)

7. Simulate (radially around the origin) a Poisson point process outside the circumcirle through the new points x_1,x_2 and x_3 (see Figure 8)

8. Create further Delaunay triangles based on this Poisson process to complete the tessellation (see Figure 9)

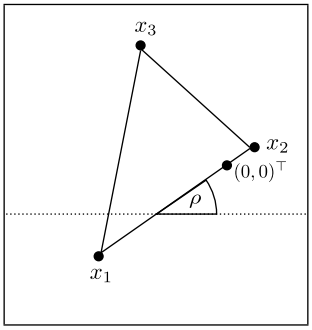

Fig. 7: Rotated and shifted triangle $\Delta(x_1, x_2, x_3)$

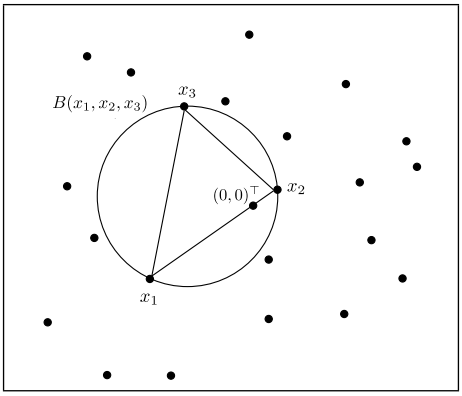

Fig. 8: Add further points

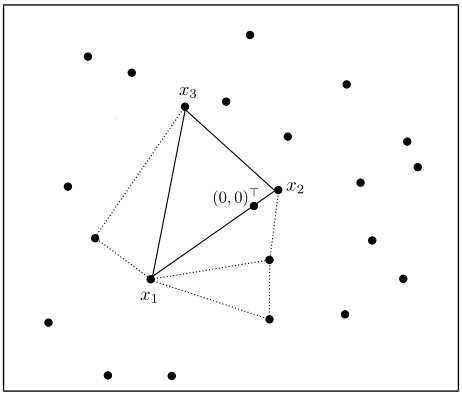

Fig. 9: Further triangles of the PDT

5 Numerical results

5.1 Comparisons of empirical densities of C^*

As already mentioned in the introduction, iterated tessellations representing the underlying infrastructure provide us, compared with simple (non-iterated)

tessellations, with much better results for potential use in models for telecommunication networks. Especially six of nine iterated tessellation types find their right to exist in this argument, namely those where the initial tessellation T_0 and the sequence of component tessellations $T_1, T_2, \ldots$ are not of the same type. Considering the remaining three types which are PVT/PVT, PLT/PLT and PDT/PDT, the mindful reader may ask himself if they are really necessary or can they be replaced by their corresponding simple (non-iterated) tessellation. To find an answer to this question, we compare empirical densities of C^* where the realisation of the typical serving zone Ξ_H^* is based on a simple tessellation, e.g. on a PLT and on the corresponding iterated tessellation, e.g. a PLT/PLT. In order to estimate $f_{C^*}(x)$, we used (3) and simulated $n = 2000$ typical serving zones Ξ_H^* containing the typical segment system S_H^* and employed the Monte Carlo estimator $\widehat{f}_{C^*}(x;n) = \lambda_\ell \, \frac{1}{n} \, \sum_{j=1}^{n} \sum_{i=1}^{M_j} \mathbb{1}_{[c(A_i^{(j)}),c(B_i^{(j)}))}(x)$ for $f_{C^*}(x)$ which was introduced in [16]. For all simulations, we set the length intensity $\gamma = \gamma_0 + \gamma_1 \equiv 1$ and write $\kappa = \frac{\gamma}{\lambda_\ell}$ for the scaling factor (for details see [7, 17]). Figure 10 shows $\widehat{f}_{C^*}(x;n)$ based on PVT (black) and PVT/PVT (gray) where $\frac{\gamma_0}{\gamma_1} = 3$, $\frac{\gamma_0}{\gamma_1} = 1$ and $\frac{\gamma_0}{\gamma_1} = \frac{1}{3}$ (from left to right). In Figure 11 and Figure 12, we display analogous results for PLT and PLT/PLT as well as for PDT and PDT/PDT, respectively. For all nine cases, we exemplarily took $\kappa = 10$. Remember that $\gamma = 1$ for the iterated and non-iterated cases. In the Voronoi case and the Delaunay case, we observe only very moderate differences between the two density functions for all three ratios of γ_0 and γ_1 (see Figures 10 and 12). In the PLT case the typical shortest path length C^* based on the scenario with iterated tessellation is clearly smaller in expectation than C^* based on the scenario with the non-iterated tessellation regarding $\frac{\gamma_0}{\gamma_1} = 3$ and $\frac{\gamma_0}{\gamma_1} = 1$ whereas for $\frac{\gamma_0}{\gamma_1} = \frac{1}{3}$, the gray density (iterated scenario) approximates the black density (non-iterated scenario) quite well. One possible reason for this different behavior in the PLT case may be related to the relative location of the HLC on S_H^*. In [12], it was observed that by using graph-based serving zones instead of Euclidean serving zones -where we can always observe a decrease of C^*- this decrease is especially pronounced in the PLT case. This indicates that the HLC lies close to the boundary of Ξ_H^* relatively frequently. Therefore, we expect that iteration reduces this effect.

Furthermore, when combining tessellations of different types, one expects clear differences for the density of C^* as can be seen in Figure 13. Besides this, we investigated the differences in the behavior of the empirical density function $\widehat{f}_{C^*}(x;n)$ of some iterated tessellation $T = \tau(T_0 \mid T_1, T_2, \ldots)$ and its reciprocal tessellation $T' = \tau(T_0' \mid T_1', T_2', \ldots)$ where $T_0' \stackrel{d}{=} T_i$ for $i \geq 1$ with length intensity $\gamma_0' = \gamma_1$ and where $T_i' \stackrel{d}{=} T_0$ for $i \geq 1$ with length intensity $\gamma_1' = \gamma_0$. This has been done in order to find out if some of these tessellation types are redundant. Figure 14 shows $\widehat{f}_{C^*}(x;n)$ based on PVT/PDT with $\frac{\gamma_0}{\gamma_1} = 3$ (black) and PDT/PVT with $\frac{\gamma_0}{\gamma_1} = \frac{1}{3}$ (gray) on the left side, whereas the right-hand side displays the empirical densities of C^* based on PLT/PVT with $\frac{\gamma_0}{\gamma_1} = 3$ (black) and PVT/PLT

with $\frac{\gamma_0}{\gamma_1} = \frac{1}{3}$ (gray). In both cases we chose $\kappa = 60$. Depending on the type of the nested iterated tessellation, we obtain either very similar, almost the same empirical density functions for C^* (on the left) or quite different ones (on the right), based on T and T', respectively.

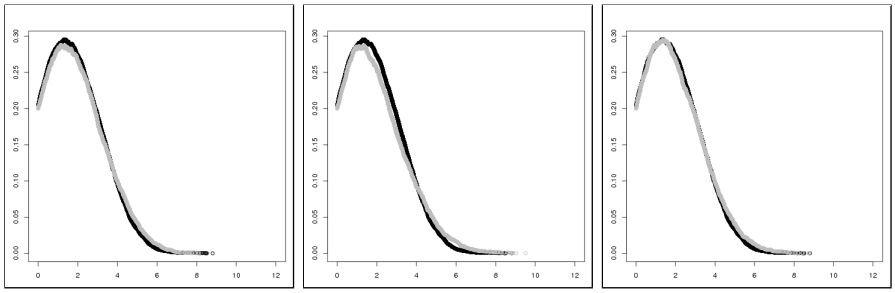

Fig. 10: $\widehat{f}_{C^*}(x;n)$ based on PVT (black) and PVT/PVT (gray) where $\frac{\gamma_0}{\gamma_1} = 3$, $\frac{\gamma_0}{\gamma_1} = 1$ and $\frac{\gamma_0}{\gamma_1} = \frac{1}{3}$ (from left to right).

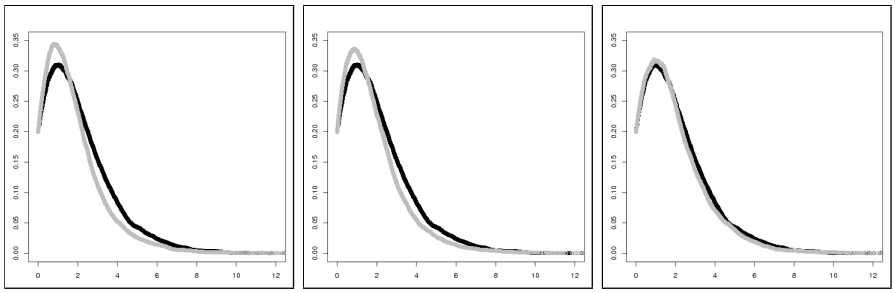

Fig. 11: $\widehat{f}_{C^*}(x;n)$ based on PLT (black) and PLT/PLT (gray) where $\frac{\gamma_0}{\gamma_1} = 3$, $\frac{\gamma_0}{\gamma_1} = 1$ and $\frac{\gamma_0}{\gamma_1} = \frac{1}{3}$ (from left to right).

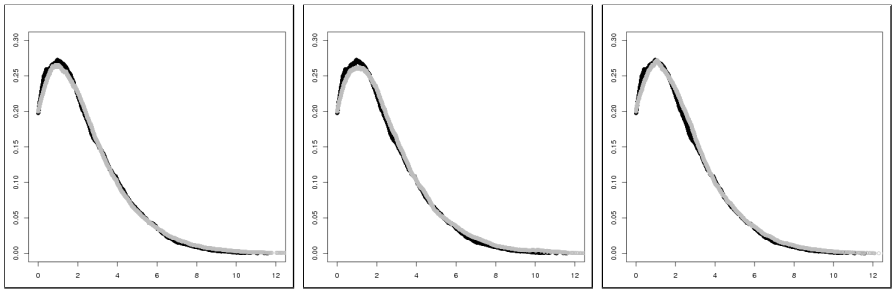

Fig. 12: $\widehat{f}_{C^*}(x;n)$ based on PDT (black) and PDT/PDT (gray) where $\frac{\gamma_0}{\gamma_1} = 3$, $\frac{\gamma_0}{\gamma_1} = 1$ and $\frac{\gamma_0}{\gamma_1} = \frac{1}{3}$ (from left to right).

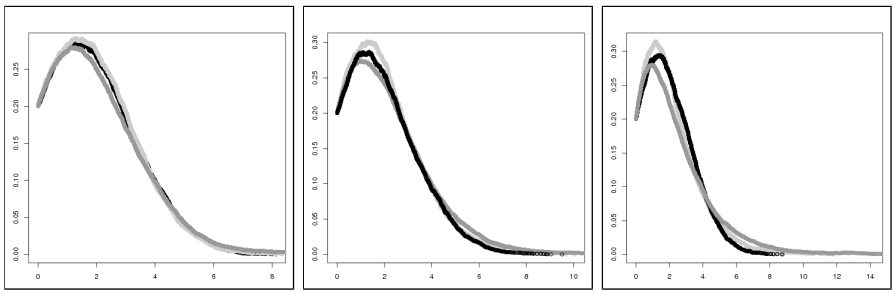

Fig. 13: $\widehat{f}_{C^*}(x;n)$ based on PVT/PVT (black), PVT/PLT (light gray) and PVT/PDT (dark gray) where $\frac{\gamma_0}{\gamma_1} = 3$, $\frac{\gamma_0}{\gamma_1} = 1$ and $\frac{\gamma_0}{\gamma_1} = \frac{1}{3}$ (from left to right).

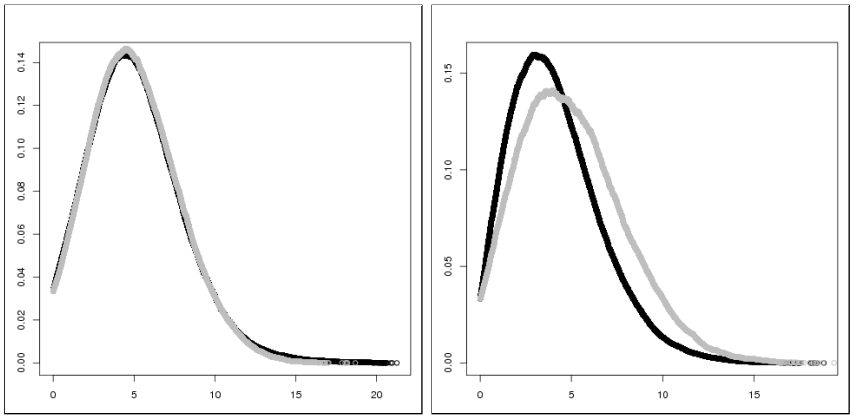

Fig. 14: $\widehat{f}_{C^*}(x;n)$ based on PVT/PDT (left) resp. PLT/PVT (right) and their corresponding reciprocals

5.2 Model choice for the distribution of typical shortest path length

Unfortunately, there exists no explicit formula for the density f_{C^*} of the typical shortest path length C^* so far. In this section, we therefore want to find an analytical function with only few parameters approximating the density of C^* based on an iterated tessellation T representing the infrastructure. Considering the shape of the empirical densities of C^* in Figure 15 as well as the limit results derived in Section 3, it seems reasonable to use truncated Weibull distributions as a family for approximative parametric distributions of C^*. In particular, it is the same family which has been applied for non-iterated tessellations, see [7],

i.e. the parametric density function $f : [0, \infty) \to [0, \infty)$ we use is given by

$$f(x) = \frac{a}{b \cdot \exp\left(-\left(\frac{2b}{\kappa a}\right)^{\frac{a}{a-1}}\right)} \cdot \exp\left(-\left(\frac{x}{b} + \left(\frac{2b}{\kappa a}\right)^{\frac{1}{a-1}}\right)^{a}\right) \cdot \left(\frac{x}{b} + \left(\frac{2b}{\kappa a}\right)^{\frac{1}{a-1}}\right)^{a-1},$$

for $x \geq 0$ where $a, b > 0$ are some parameters. Note that we can apply this family of parametric distributions for all nine possible cases of nested iterated tessellations based on PLT, PVT and PDT. In Figure 15, we display the empirical density of C^* (gray) together with the fitted Weibull density (black) where on the left hand side the infrastructure is represented by PVT/PDT with $\kappa = 30$ and $\frac{\gamma_0}{\gamma_1} = 1$ whereas on the right hand side the road system is modeled by PDT/PLT with $\kappa = 120$ and $\frac{\gamma_0}{\gamma_1} = \frac{1}{3}$.

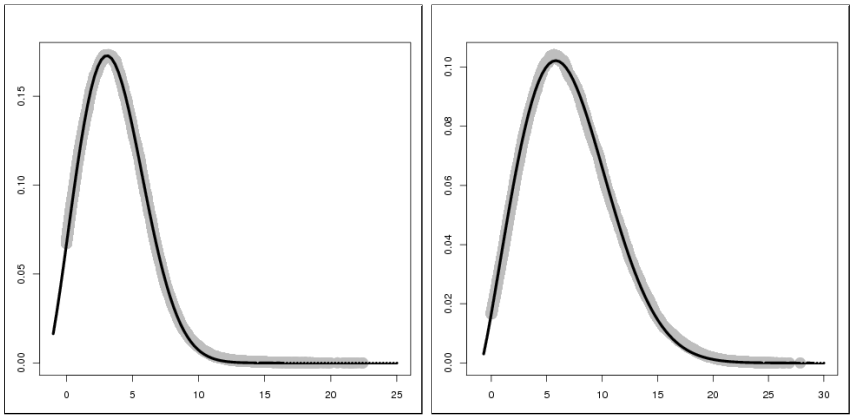

Fig. 15: Empirical densities for C^* (gray) and corresponding fitted Weibull densities (black)

6 Conclusions

We show that as $\gamma_0 \to 0$ and $\gamma_1 \to 0$, the distribution of the typical shortest path length C^* based on an iterated tessellation converges to the distribution of the typical shortest path length C^*_{comp} and C^*_{init}, respectively. In this context, we can consider a non-iterated tessellation as a special case of an iterated tessellation. In general, i.e. if neither γ_0 nor γ_1 is close to 0, analytical formulas for characteristics related to Cox-Voronoi cells are not known. Therefore, we derive an explicit description of the Palm version of a stationary Poisson-Delaunay tessellation. Combined with a simple acceptance-rejection scheme, it provides us with a new direct simulation algorithm for the Palm version of a PDT which can be used to obtain the Palm version T^* of an iterated nested tessellation T where a PDT is involved. This is an important improvement of the *SSLM* since we can now combine PVT, PLT and PDT in iterated tessellations as representation for the underlying infrastructure. We obtain much more flexibility than we

had before by only using simple (non-iterated) tessellations. Finally, the family of parametric distributions for point-to-point distances in telecommunication networks obtained in [7] turns out to provide a good fit in case that the road system is represented by iterated tessellations. Knowing the parameters a and b for all κ and all ratios $\frac{\gamma_0}{\gamma_1}$, we can avoid time consuming simulations or network reconstructions in the future and efficiently analyse networks.
For future work, it would be also interesting to develop simulation algorithms for the typical cell Ξ_H^* and the typical segment system S_H^* based on further models like Crack-STIT tessellations (see [11]) which would extend our wide range of good fits for distance distributions observed in real networks.

Acknowledgement

This work was supported by Orange Labs through Research grant No. 46146063-9241. Christian Hirsch was supported by a research grant from DFG Research Training Group 1100 at Ulm University.

References

[1] A. Baddeley, I. Bárány, R. Schneider and W. Weil. *Stochastic Geometry* Springer, Berlin, Heidelberg, 2007.

[2] V. Baumstark, G. Last, *Some distributional results for Poisson-Voronoi tessellations*, Advances in Applied Probability 39 (2007), 16-40

[3] D.J. Daley and D. Vere-Jones. *An Introduction to the Theory of Point Processes.* Vol. I/II, Springer, New York, 2005/08.

[4] F. Fleischer, C. Gloaguen, V. Schmidt and F. Voss, *Simulation of the typical Poisson-Voronoi-Cox-Voronoi cell*, Journal of Statistical Computation and Simulation 79 (2009), 939-957.

[5] C. Gloaguen, F. Fleischer, H. Schmidt, and V. Schmidt, *Simulation of typical Cox-Voronoi cells, with a special regard to implementation tests*, Mathematical Methods of Operations Research, 62 (2005), 357-373.

[6] C. Gloaguen, F. Fleischer, H. Schmidt and V. Schmidt, *Fitting of stochastic telecommunication network models via distance measures and Monte-Carlo tests*, Telecommunication Systems, vol. 31, pp. 353 377, 2006.

[7] C. Gloaguen, F. Voss and V. Schmidt, *Parametric distributions of connection lengths for the efficient analysis of fixed access networks*, Annals of Telecommunications 66 (2011), 103-118.

[8] J. Illian, A. Penttinen, H. Stoyan, and D. Stoyan. *Statistical Analysis and Modelling of Spatial Point Patterns.* J. Wiley & Sons, Chichester, 2008.

[9] D.P. Kroese, T. Taimre and Z.I. Botev. *Handbook of Monte Carlo Methods.* J. Wiley & Sons, Chichester, 2011.

[10] I.S. Molchanov. *Theory of Random Sets.* Springer, London, 2005.

[11] W. Nagel, V. Weiss, *Crack STIT tessellations: characterization of stationary random tessellations stable with respect to iteration*, Advances in Applied Probability, 37 4 (2005), 859-883.

[12] D. Neuhäuser, C. Hirsch, C. Gloaguen and V. Schmidt, *On the distribution of typical shortest-path lengths in connected random geometric graphs*, Queueing Systems 71 (2012), 199-220.

[13] R. Schneider and W. Weil. *Stochastic and Integral Geometry.* Springer, Berlin, 2008.

[14] D. Stoyan, W.S. Kendall, and J. Mecke. *Stochastic Geometry and its Applications.* J. Wiley & Sons, Chichester, 1995.

[15] F. Voss, C. Gloaguen, F. Fleischer and V. Schmidt, *Distributional properties of Euclidean distances in wireless networks involving road systems*, IEEE Journal on Selected Areas in Communication 27 (2009), 1047-1055

[16] F. Voss, C. Gloaguen, F. Fleischer and V. Schmidt, *Densities of shortest path lengths n spatial stochastic networks*, Stochastic Models 27 (2011), 141-167

[17] F. Voss, C. Gloaguen and V. Schmidt, *Palm calculus for stationary Cox processes on iterated random tessellations*, Proceedings of WiOpt2009: 7th Intl. Symposium on Modeling and Optimization in Mobile, Ad Hoc, and Wireless Networks, Seoul 2009.